

Hund's coupling driven nature of magnetism in negative charge transfer material, SrCoO₃

Jyotsana Sharma^{1,3,*}, Shivani Bhardwaj¹, and Sudhir K. Pandey^{2†}

¹*School of Physical Sciences, Indian Institute of Technology Mandi, Kamand - 175075, India*

²*School of Mechanical and Materials Engineering,
Indian Institute of Technology Mandi, Kamand - 175075, India and*

³*Swami Vivekanand Govt. College Ghumarwin - 174021, India*

(Dated: December 14, 2025)

In this work, we investigate the microscopic origin of magnetism in SrCoO₃ by incorporating electronic correlations within the dynamical mean-field theory (DMFT) framework. We note a remarkable agreement of the calculated magnetic observables (saturation magnetization $\sim 2.4 \mu_B$; magnetic transition temperature, $T_c \sim 350$ K) with the experimental results. The system exhibits Hund's coupling-induced strong quasiparticle mass enhancements of upto $m^*/m \sim 7$ for Co 3d states, with the largest renormalization occurring in the majority spin t_{2g} orbitals, marking the onset of orbital-selectivity. Our results reveal a Stoner-like collapse of exchange splitting that drives the loss of long-range ferromagnetic order at T_c . The breakdown of Fermi-liquid behavior down to $T \sim 100$ K suggests a suppressed coherence scale. Local magnetic moment originates from a mixed-spin configuration formed through dynamical fluctuation between intermediate-spin and high-spin states. Large charge fluctuations ($\langle \Delta N^2 \rangle \sim 0.6$) together with heavy quasiparticles establish the correlation effects regime, governed predominantly by Hund's physics in SrCoO₃.

I. INTRODUCTION

The transition metal oxides belonging to the Ruddlesden-Popper (RP) series ($A_{n+1}B_nO_{3n+1}$) offer a variety of unconventional electronic and magnetic phenomena arising from strong correlations, reduced dimensionality, and interplay between lattice, charge, and spin degrees of freedom[1–6]. The end-member ($n = \infty$) perovskites (ABO₃) are of particular significance as they represent the bulk three-dimensional limit of the RP series. The end-members of the homologous series majorly establish the foundation of the electronic structure, charge-transfer behavior, metal-ligand coupling etc. of the correlated-electron properties of the RP members with reduced dimensionality ($n=1,2,3,\dots$)[7–10].

The ABO₃ perovskites have been extensively studied and found to exhibit phenomena of fundamental interest such as correlated metallicity, negative charge-transfer physics, spin-state transitions, structural transitions, ferroelectricity, colossal magneto-resistance, unconventional magnetism, superconductivity, large thermopower, spin-glass behaviour, metal-insulator transition etc.[11–18]. These end-members are largely comprised of systems that show paramagnetic metallic states (e.g., LaNiO₃, SrVO₃) or antiferromagnetic insulating states (e.g., LaFeO₃, LaMnO₃, SrMnO₃). However, among these, SrCoO₃ occupies a unique position as it remains cubic without any distortion and is one of the few transition-metal perovskites -together with SrRuO₃- that stabilizes in a ferromagnetic ground state with remarkably high Curie temperature ($T_c \sim 305$ K)[19] for single-crystal sample, far exceeding its ruthenate counterpart ($T_c \sim 160$

K)[20].

The available experimental literature on the stoichiometric SrCoO₃ is limited primarily due to the difficulty associated with preparing samples with negligible oxygen deficiency[21, 22]. Nevertheless, the experimental measurements report that saturation magnetization ($2-2.5 \mu_B$) lies close to the intermediate-spin (IS) state ($S = 3/2$)[23], rather than the usually expected low-spin (LS) or high-spin (HS) ground state configurations. The earliest of studies proposed an IS ($S = 3/2$) ground state ($3\mu_B$) as the natural explanation for the observed experimental magnetic moment of SrCoO₃, attributing it to the strong ligand hole coupling[24]. The majority of previous theoretical work on SrCoO₃ has been limited to static-mean field approaches[21, 23, 25], such as DFT or DFT+ U , which fail to capture the dynamical fluctuations among LS, IS and HS multifold and correlation effects, crucial for characterizing covalent Cobaltate systems. Moreover, a precise description of the effective spin state for the system resulting from the competition between the crystal field effects and Hund's coupling (J) would require a realistic account of J (correspondingly, Hubbard U) since the crystal field limit is, to an extent, better captured by the static mean-field treatments.

The only study available with the dynamical many-body treatment (DFT+DMFT) for SrCoO₃ is by Kunes et al[24], which claims the ground state effective spin of SrCoO₃ does not stem from a pure ionic configuration but rather from a superposition of different atomic spin states. They also propose a plausible double-exchange mechanism for magnetism, attributing it to the presence of a mixed-valence Co 3d configuration. However, these results are obtained for a Hubbard U value of ~ 10 eV, which is unusually high for a metallic system. Their calculations show a remarkably high T_c (~ 1800 K), which is likely due to the density-density approximation

* jyotsana.sharma1290@gmail.com

† sudhir@iitmandi.ac.in

of the Coulomb interaction form adopted in their work, as it suppresses the spin-flip and pair hopping terms essential for a realistic description of the spin fluctuations. The non-density-density terms become particularly more important for the accurate account of low-energy excitations and quasiparticle renormalization[26].

Furthermore, a recent experimental and DFT+DMFT investigation on highly strained SrCoO₃ thin films[27] revealed that ferromagnetism persists even across a strain-induced metal-insulator transition, indicating that the unexpectedly strong ferromagnetism observed in unstrained pure SrCoO₃, likewise originates from a correlation-driven mechanism rather than classical Zener double-exchange physics. These studies suggest the presence of an interesting magnetic phase in the SrCoO₃ driven by its spin state and strong covalence effects, as reported in the system, which includes negative charge transfer. Therefore, an advanced beyond-static mean-field treatment is necessary, considering the current advancements in the field, which include the accurate first-principles determination of Coulomb interaction parameters (U and J) as well as the full Coulomb interaction matrix, to gain microscopic insights into the fundamental nature of its magnetic spin state and spectral properties. In this paper, we systematically examine the role of correlation effects in determining the magnetism and spectral properties of SrCoO₃, using first-principles-determined Hubbard U and Hund's coupling J . We observe a Hund's-dominated description of magnetism present in the system, stabilizing in a mixed spin state configuration comprised primarily of IS and HS configurations. The system exhibits evidence of strong quasiparticle mass enhancements with a largely suppressed orbital-selective coherence scale.

II. COMPUTATIONAL DETAILS

To understand electronic structure of SrCoO₃, we initially performed first-principle DFT calculations using APW+lo based WIEN2k code [28]. The PBEsol[29] exchange-correlation functional under GGA approximation has been used. The initial structural details were taken from XRD data for SrCoO₃[19]. The lattice parameter was optimised using volume optimisation tool in Wien2k. All calculations were performed over a mesh size of 12x12x12 keeping RMTKmax equal to 7. The RMT values for Sr, Co and O were taken as 2.30 au, 1.87 au and 1.61 au respectively. The convergence criteria was set for charge at 10^{-4} Coulomb/cell. Both non magnetic (NM) and spin-polarised (SP) calculations were performed. The Gap2c[30] code is used for the constrained random phase approximation (cRPA) calculations to determine the partially screened Coulomb interaction parameters (U and J) to be used for the DFT+DMFT calculations. Further, the value of U has also been estimated via linear response method as im-

plemented in the Abinit code[31][32]. The linear response method in Abinit computes U by measuring the change in orbital occupation on applying small local potential shifts. The DFT+DMFT calculations have been performed using the eDMFT[33] code. Here impurity model of DMFT is solved for $U = 6.0$ eV and $J = 1.15$ eV using CTQMC (continuous-time Quantum Monte Carlo) impurity solver. The results are obtained for various exact double-counting (DC) schemes[34] available in the eDMFT code. The spin-rotational invariant (*full*) form of local Coulomb interaction is used for solving the DMFT impurity solver for realistic account of electronic interactions. A hybridization window ranging from -15 eV to 15 eV has been chosen for the DFT+DMFT calculations.

III. RESULTS AND DISCUSSIONS

SrCoO₃ is known to possess simple cubic $Pm\bar{3}m$ structure[19]. The atoms Sr, Co and O are located at Wyckoff positions 1b (0.5,0.5,0.5), 1a (0,0,0) and 3d (0.5,0,0) respectively. The Co atom is surrounded by a regular octahedron of Oxygen ligands. This cubic octahedral geometry splits Co-3d orbitals into triply degenerate $t_{2g}(d_{xy}, d_{yz}, d_{zx})$ and doubly degenerate $e_g(d_{3z^2-r^2}, d_{x^2-y^2})$ orbitals. To investigate the electronic structure in detail, we first performed lattice parameter optimization for our system. We calculated total energy of the system at different unit cell volumes. The total energy vs. volume per unit cell curve is shown in Fig. 1. This plot is then fitted with Birch-Murnaghan equation of state[35] to obtain volume corresponding to minimum total energy. The obtained volume from fitted curve is 364.41 a₀³. This volume gave lattice constant value $a = 3.7798$ Å. The fitting of total energy vs. volume data also provides bulk modulus B_0 and its first pressure derivative B'_0 . All these ground state material parameters calculated using PBEsol approximation are summarized in Table I along with results from previous theoretical and experimental works. Our calculated values agree fairly with the theoretical works of Ali & Ahmad[36] performed using Wu-Cohen GGA. On comparing the experimental value of lattice constant, 3.8289 Å[19] taken at room temperature, with our calculated value of 3.7798 Å which is at 0 K; we get a thermal expansion coefficient of $\sim 4.2 \times 10^{-5}$ K⁻¹. This value of thermal expansion coefficient agrees with those from previous work[37]. Hence, we can say our calculated value of lattice constant is consistent with the experimental results. Thus, the comparison of our present work with the previous works, ascertains that PBEsol exchange correlational functional works reliably for this compound. We have used the volume-optimized calculated value of lattice parameter in this study throughout.

From DFT calculations, total magnetic moment came out to be 2.50 μ_B /f.u.. The magnetic moment contribution from within muffin tin of Co is 1.83 μ_B ,

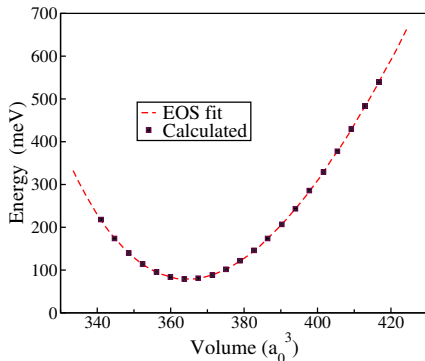


FIG. 1: Energy vs. Volume per unit cell

TABLE I: Calculated material parameters lattice constant a , bulk modulus B_0 and its first pressure derivative B'_0 for SrCoO₃ compared to previous theoretical and experimental results

Parameters	Present Work	Previous Theoretical	Experimental
a (Å)	3.7798	3.78[36]	3.8289[19] 3.8246[38]
B_0 (GPa)	173.57	176.14[36], 144[11]	-
B'_0 (GPa)	4.95	5.32[36], 4[11]	-

Ref.[36] used Wu-Cohen GGA [39] as implemented in WIEN2K
 Ref.[11] used GGA as implemented in VASP[40]

O is 0.18 μ_B and interstitial is 0.13 μ_B . The finite magnetic moment on Oxygen atoms indicates the possibility of negative charge transfer[23, 41] from O-2p to Co-3d resulting in unpaired electron and hence, the covalent contributions to the bonding in SrCoO₃. The experimental value of low temperature moment for single crystal stoichiometric SrCoO₃ at 2 K is 2.5 μ_B /f.u.[19] when 7 T magnetic field is applied. The calculated magnetic moment value comes out to be in good agreement with the experimental[19] and previous theoretical[21, 25] results (tabulated in Table II).

Since SrCoO₃ is a strongly correlated system, we employed DFT + DMFT approach to incorporate correlation effects into our study of the magnetization of SrCoO₃ as a function of temperature. The predictive power of DMFT depends majorly on Coulomb interaction parameters U and J as these parameters account for strength of correlations among electrons. Different DFT+ U studies have employed various U values for SrCoO₃ such as 2.5[43] eV, 2.75[44] eV, 7.0[45] eV. We found only one DFT+DMFT study by Kunes et. al. [24], where $U = 10.83$ eV and $J = 0.76$ eV has been used but this value is too high for a metallic system. In this work we performed constrained random phase

TABLE II: Total magnetic moment of SrCoO₃ compared to previous theoretical and experimental results

Parameters	Present Work	Previous Theoretical	Experimental
μ_{total} (μ_B /f.u.)	2.50	2.45[36], 2.28[21]	2.5[19]
μ_{Co} (μ_B /atom)	1.83	1.79[36], 1.69[25]	1.78[42]
μ_O (μ_B /atom)	0.18	0.17[36], 0.19[25]	-
$\mu_{interstitial}$ (μ_B)	0.13	0.15[36]	-

Ref.[36] used Wu-Cohen GGA [39]

Ref.[21] used GGA+U (with $U_{eff} = 5eV$)

Ref.[25] used von Barth–Hedin exchange correlation

approximation (cRPA) calculations to determine the Coulomb interaction parameters U . Since cRPA has different tweaking parameters and the values of Coulomb interaction parameters are known to be sensitive to various factors such as the choice of correlated energy window, number of correlated bands, choice of projectors used for constructing Wannier functions etc.[46, 47], therefore, we have studied the variation in the values obtained depending on the number of bands constituting the correlated subspace to determine realistic U for the DFT+DMFT calculations. The resulting values are tabulated in Table III, where U_{full} (U_{diag}) denote the averages of the all (diagonal) matrix elements of the effective Coulomb interaction matrix. Firstly, all 14 bands in the energy window ranging from -7.5 eV to 4 eV, are selected for constructing maximally-localized Wannier functions, because, strong hybridization of Co- d and O- p states leads to largely entangled d -character bands as shown in Fig.2. Then we performed calculations with different number of bands masked to constrain the intra-3d transitions. This results in large value of $U_{full} \sim 12$ eV and a similar order of U_{diag} . However, further excluding the 1st and 2nd bands from the correlated subspace leads to largely reduced U ($U_{full} \sim 7$ eV and $U_{diag} \sim 8$ eV) suggesting large screening effects from the 1st and 2nd bands. With further exclusion of the bands and considering the range of constrained bands as 4-14, 5-14 and 6-14, results in reduction of U (U_{full}) values to ~ 6.16 eV, 5.41 eV and 4.86 eV, respectively. Note that the range selected with bands 4-14, is characterized by dominant Co 3d character relative to other bands and yield a value of U around 6 eV. Furthermore, we find that this value comes in close agreement with the linear response calculated U ($U=5.95$ eV) (refer Table III). We therefore used $U=6.0$ eV in the DFT+DMFT calculations with J (correspondingly deduced from Yukawa screening method) = 1.15 eV for SrCoO₃.

We next examined the robustness of our results against the choice of different DC schemes (i.e. *exactd*, *exact*,

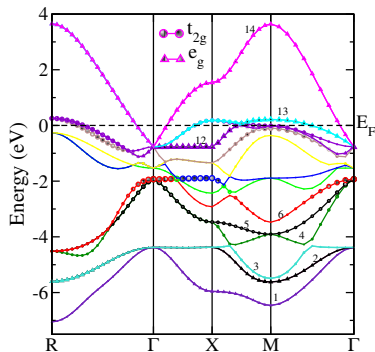


FIG. 2: Band character plot of Co-3d orbitals in NM phase obtained at DFT level.

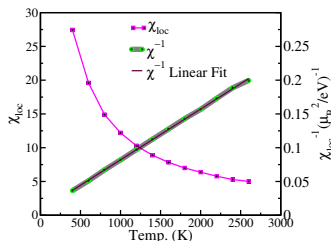


FIG. 3: Temperature dependent local spin susceptibility (χ_{loc}) obtained in the paramagnetic phase above T_c along with the inverse χ_{loc} and its Curie-Weiss fit.

exactly) by evaluating the variation in saturation magnetization value as given in Table. IV). Among the given DC schemes, *exactly* gives the value of saturation magnetization $\sim 2.44 \mu_B$, exceptionally close to the experimental value of $2.50 \mu_B$ [19]. Moreover, the *exactly* DC scheme provides the magnetic transition temperature (T_c) of ~ 350 K, which lies in remarkable match with the experimental value of 305 K. This is consistent with the previous results of the metallic systems for which *exactly* is found to be more suitable DC scheme[5, 34]. Thus, *exactly* DC scheme is adopted throughout the study.

Fig. 3 depicts the local spin susceptibility (χ_{loc}) and its inverse (χ_{loc}^{-1}), in the paramagnetic phase above T_c . The χ_{loc}^{-1} shows an appreciably linear behavior over a large range of temperature (500-2500 K), indicating the presence of unscreened local moments in the paramagnetic phase of SrCoO₃. We find the local magnetic moment from the linear slope of χ_{loc}^{-1} by fitting as:

$$\chi_{loc}^{-1} = 3(g\mu_B)^2(T + T_w)/\mu_{loc}^2$$

where $g = 2$, and T_w is the Kondo temperature.

TABLE III: ab-initio calculation of Coulomb interaction parameters. U in the units of eV

ab-initio method	index of bands masked	U_{full}	U_{diag}
cRPA	1-14	12.20	12.54
	3-14	7.02	8.2
	4-14	6.16	7.41
	5-14	5.41	6.63
	6-14	4.86	6.06
Linear Response	-	5.95	-

TABLE IV: Values of saturation magnetization obtained using different dc schemes for $U_{full} = 6$ eV

dc scheme	$\mu_B/\text{f.u.}$
exactd	1.68
exact	1.88
exactly	2.44

The fit yields a local moment value of ($\mu_{loc} \sim 3.21 \mu_B$, representing an effective spin state of $S = 1.2$ ($2.4 \mu_B$). This estimated value comes in quite good agreement with the observed saturation magnetization of SrCoO₃ in the experimental reports ($\sim 2.5 \mu_B$). The overall remarkably good agreement of the calculated T_c and the low temperature magnetization ($2.44 \mu_B$) from the single-site DMFT, reflects a Hund's dominated description of magnetism in this system.

Next, the effect of electronic correlations on the spectral properties of SrCoO₃ is presented. Fig. 4 (i) shows spin-orbital resolved DFT+DMFT PDOS computed at 110 K alongwith DFT PDOS. The inclusion of correlation effects introduces notable changes with respect to the DFT. Firstly, for all Co-3d states, new incoherent features appear at higher binding energies ($\sim 8-10$ eV below E_F) where DFT PDOS is negligible and the low-energy quasiparticle states become narrower. We can observe that peaky structures form in the DFT+DMFT PDOS for both t_{2g} and e_g orbitals, marking significant renormalization of the DFT PDOS due to correlation induced smearing of states. The system exhibits an orbital-dependent polarization at E_F with t_{2g} states dominating the minority and e_g orbitals dominating the majority spin-channels. The t_{2g} -up states show a gap formation (Mott-like localization) in the DFT+DMFT PDOS (refer inset of part (a) of Fig. 4 (i)), as incoherent weight starts to appear above the E_f . On the contrary the DFT PDOS of t_{2g} -up states lie almost fully occupied below the E_f (clearly visible from the absence of DFT PDOS in very close proximity of the E_F :inset of part (a) Fig 4 (i)). The t_{2g} -dn sector shows quite small renormalization of DFT PDOS, which is evident from a similar spectral weight distribution as that of its DFT PDOS around the E_f , also relatively robust bandwidth

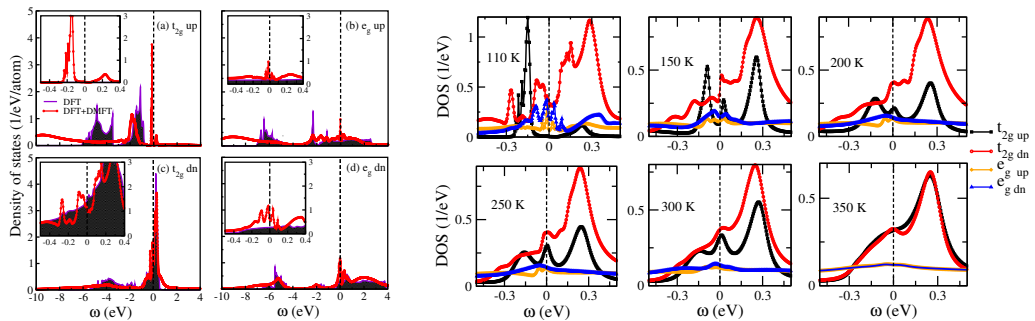


FIG. 4: (Right)(i) Spin and orbital resolved DOS plot obtained from DFT (shaded) and DFT+DMFT at 110 K (unshaded) for t_{2g} and e_g orbitals. Dashed line at $\omega = 0$ represents E_f . (Left)(ii) Temperature-dependent evolution of the spin-orbital resolved DOS below T_c in the vicinity of E_f at DFT+DMFT level.

against correlations and thermal effects (refer figure 1. of supplemental material). Here the results point to majorly localized nature of the t_{2g} sector. The e_g orbitals display formation of major quasiparticle spectral weight around the E_F in both their majority and minority spin channels, resulting from their itinerant character. The low energy normalization of PDOS obtained after treatment with dynamical correlations suggest evolution of DOS into a spin-orbital selective Mott-like localization at low temperature.

Further, to study the evolution of quasiparticle spectral weight distribution across the FM phase, its temperature dependent evolution of spectral density of Co $3d$ states is given in Fig. 4 (ii). The presence of quasiparticle peaks is noted at low temperatures $T \sim 110$ K for the e_g sector, which eventually lose coherence upon increasing the temperature to 200 K and above, suggesting a coherence scale of around 100 K. While the majority t_{2g} sector is localized and minority sector shows largely broadened quasiparticle peak at E_f , suggesting even lower temperature coherence scale than 110 K. As the temperature is increased both the t_{2g} and e_g sectors undergo significant thermal broadening of the quasiparticle states, where the e_g sector loses coherence more rapidly among the two, which is visible from the significant broadened weight of e_g states at $T=150$ K. Correspondingly, the Hund's exchange splitting in the e_g manifold collapses ~ 250 K, significantly earlier than in the t_{2g} channel, where the exchange splitting persists upto T_c . Interestingly, at 150 K the t_{2g} -dn orbital shows a diverging behavior at the E_f , due to a possible presence of Van-Hove singularity at finite temperature, signature of which is also present as slight increase in its scattering rate value (which will be discussed later in the text; refer Fig. 5). Also the peak of t_{2g} -up DOS at ~ -0.15 eV splits into two peaks, leading to disappearance of gap at the E_f which appears in the form of a pseudogap like feature, as the temperature is increased to 150 K. Overall, the exchange splitting, dominated in magnitude by the t_{2g} states,

decreases approximately in proportion to the net magnetization. The principal collapse of exchange splitting sets in around ~ 300 K, close to the experimental Curie temperature of SrCoO₃. This seems consistent with the Stoner-like description of the itinerant ferromagnetic transition. Notably, this behavior contrasts with that of SrRuO₃ where finite exchange splitting survives even at the magnetic transition temperature[20], suggesting more degree of itinerant nature of magnetism in SrCoO₃ than its ruthenate counterpart.

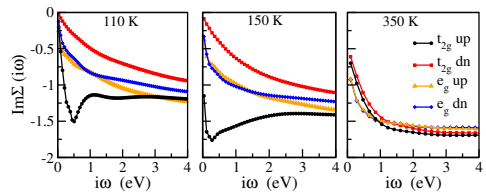


FIG. 5: Variation of spin-orbital resolved imaginary part of self-energy ($Im\Sigma(i\omega)$) in Matsubara frequency below T_c .

Next, the quasiparticle broadening of the Co $3d$ states is quantified by the imaginary part of self-energy obtained in the Matsubara frequency regime. In Fig.5, the temperature evolution of imaginary parts of self-energy ($Im\Sigma(i\omega)$) of the t_{2g} and e_g orbitals are shown on the imaginary frequency axis. It is clearly seen that at low energies, the behavior of $Im\Sigma(i\omega)$ is qualitatively different for t_{2g} and e_g orbitals and there is further level of spin-polarized distinction within the t_{2g} manifold. This also marks the onset of orbital selective Fermi-liquid coherence scale in the system, a characteristic signature of Hunds induced correlations. At low temperatures ~ 110 K, while the $Im\Sigma(i\omega)$ of t_{2g} -dn state shows linearly vanishing behavior at low-frequency region consistent with Fermi liquid behavior, the t_{2g} -up states exhibit a diver-

gent behavior (non-linear) near the low imaginary frequency region ($i\omega=0-1$ eV) indicating strong deviation from the Fermi-liquid behavior and signature of Mott-like localization of the t_{2g} - up state, as discussed in the earlier section. The e_g orbital shows nearly Fermi-liquid like behavior in both its majority and minority spin-channels with quite small values of scattering rate (~ 0.15 eV) for each channel at 110 K. As the temperature is increased to 150 K, the behavior remains same except that the $Im\Sigma(i\omega)$ curve of the t_{2g} - dn state gains finite intercept towards zero Matsubara frequency showing finite quasiparticle lifetime and slightly increased scattering rate. However, the t_{2g} - up state shows an enlarged scattering rate at 150 K (~ 1.2 eV). On the other hand, the scattering rate of e_g orbital for both spin- up and spin- dn channels remain relatively unaffected as the temperature is increased to 150 K. However, around T_c at $T=300$ K, the curves of $Im\Sigma(i\omega)$ of both the spin channels of t_{2g} orbitals overlap at ~ 0.65 eV, which results from reduced scattering rate value for the t_{2g} - up channel resulting from appearance of finite spectral weight at E_f after disappearance of gap and increased scattering rate for the t_{2g} - dn channel, due to increased temperature dependent incoherence in t_{2g} - dn channel. Similarly, overlap in values is noted for the e_g - up and e_g - dn states at slightly large intercept (~ 1 eV). This is likely due to collapse of spin-polarization.

Correspondingly, the mass enhancement factor Z^{-1} , which is the ratio of effective mass (m^*) of interacting electron to the mass of non-interacting electron (m_{DFT}), is calculated as :

$$Z^{-1} = 1 - [\delta Im\Sigma(i\omega)/\delta\omega]_{0+} \quad (1)$$

Table V. shows spin-orbital resolved mass enhancements for Co $3d$ states at the lowest calculated temperature i.e. 110 K against the variation in the strength of J (0, 0.6, 1.15 eV). At $J=0$ eV, the t_{2g} and e_g sector show nearly coherent character with $Z\sim 0.7-0.8$, with slight mass enhancement for each sector. While increasing the J value to 0.6 eV, a modest differentiation between the orbitals begins, especially the t_{2g} - up ($Z^{-1}=2.44$) and eg - up ($Z^{-1}=2.00$) sector gains relatively moderate mass enhancement relative to their spin-dn counterparts. However, at $J=1.15$ eV, which is the value of Hunds coupling benchmarked for the system, we observe drastic rise in the mass enhancement factor ($m^*/m_{DFT}\sim 6-7$) characterized by strong orbital differentiation. (Note that from the above discussion of the scattering rate behavior at $J=1.15$ eV, the t_{2g} - up states show non-Fermi liquid behavior even at 110 K and hence quasiparticle picture breaks down. Therefore, for the t_{2g} - up states the first few Matsubara frequencies are considered for calculating the Z^{-1} , i.e. first six Matsubara frequency points, where the $Im\Sigma(i\omega)$ can be linearly approximated). Interestingly, the largest mass renormalization Z^{-1} (m^*/m_{DFT}) = 7.13 is obtained for the $t_{2g} - up$ states. Whereas, the spin- dn counterpart of the t_{2g} states, undergoes a relatively small mass renor-

malization of ~ 1.88 , which is expected since this channel experiences relatively less effective correlation induced renormalization due to large bandwidth and subsequent Fermi-liquid like behavior as mentioned in earlier. The e_g sector also shows large mass enhancement values in both its spin-channels (e_g - $up\sim 6.24$; e_g - $dn\sim 5.46$), which is surprisingly nearly same as that of the t_{2g} - up states, inspite of largely Fermi-liquid behavior at 110 K.

Unlike t_{2g} - up states, the t_{2g} - dn sector majorly stays robust against the variation in J , which reflects spin-polarized nature of correlation effects defining the t_{2g} sector. The strong quasiparticle mass renormalization for the t_{2g} - up (> 6) and e_g (> 5) states at $J=1.15$ eV result from Hunds-driven correlations in the system. These values are significantly larger than the mass enhancement observed for its Ruthenate counterpart i.e. SrRuO₃ ($m^*/m_{DFT}\sim 4$), where it is attributed to strong coupling to the low-energy bosonic modes arguing weaker electronic correlation effects[20]. However, here in the case of SrCoO₃, the large mass enhancement results from electronic correlations. We also quantify the charge fluctuations ($\langle\Delta N^2\rangle$) at $J=1.15$ eV and find the value to be ~ 0.62 at 110 K and remains almost the same throughout the FM phase showing temperature independent variation. The substantial value of $\langle\Delta N^2\rangle$ suggests a predominantly competing degree of itineracy of Co $3d$ electrons as also observed for recently reported value ~ 0.6 for $n=1$ member of RP series i.e. Sr₂CoO₄[5]. The large orbital differentiated intermediate mass enhancement values accompanied by significant charge fluctuations mark onset of Hunds metal characteristics in multiorbital systems[48-50].

We further present the finite temperature atomic-multiplet probabilities of the Co $3d$ states (Fig.6) and note that the occupation probabilities remain nearly temperature independent. The Co $3d$ orbitals show a mixed-valence state with the largest probability corresponding to the $3d^6$ multiplet, suggesting the ground state with large probability of the d^6 occupancy. The d^5 , d^7 multiplets also show significantly finite probabilities, with d^7 being $\sim 60\%$ of the d^6 probability leading to a mixed valence state indicating large covalency effects resulting from strong ligand hybridization. Interestingly, the presence of mixed-valence state of Co $3d$ orbital has been previously also noted by Kunes et. al.[24], proposing a plausible double-exchange (DE) mechanism of ferromagnetism in the system. However, our results using *full* rotationally invariant form of Coulomb interaction do not support DE-driven ferromagnetism in SrCoO₃, since we obtain a qualitatively different picture of low-energy coherence in Co- $3d$ manifold. For DE to be relevant, the orbitals which mediate the hopping (typically the e_g states) should maintain sufficient quasiparticle coherence for ensuring spin alignment between the neighboring Co (impurity) sites. On the contrary, our results show strong quasiparticle mass renormalization leading to largely suppressed Z (<0.2) factor for both the spin-channels of e_g

orbitals. These Z values indicate the presence of incoherent and heavy carriers. Therefore, the long-range coherent hopping required for a robust DE mechanism is expected to be suppressed. This assessment is further evident from the spin-orbital resolved scattering rates (from the $Im\Sigma(i\omega)$), which remain large at the lowest calculated temperature $T=110$ K for both the spin channels of e_g orbitals. Therefore, the mixed-valence in $SrCoO_3$ signals strong covalency effects rather than a functional DE mechanism.

We systematically examine the electronic occupancies of the t_{2g} and e_g states to establish the role of correlation effects in deciding the spin-state configuration of the Co $3d$ states in $SrCoO_3$. Table VI shows the orbital and spin resolved occupancies of the Co $3d$ states obtained at the DFT level and also the occupancies obtained on employing the dynamical correlation effects using DFT+DMFT (at 110 K). The degree of correlations can be found based on the partial charges of Co $3d$ electrons within DFT+DMFT in comparison to DFT. The DFT calculated occupancy of the Co $3d$ orbital adds upto ~ 6.41 , whereas, in the DFT+DMFT calculations it is found to be ~ 6.27 (at $J=1.15$ eV). This modest reduction of the partial charge by $\sim 0.14e$ hints to a moderately correlated regime with not so strongly suppressed charge-fluctuations, consistent with the above noted conclusion from $\langle \Delta N^2 \rangle$ value. This stands in contrast to the previously reported large partial charge renormalization upto $\sim 1e$, which should be interpreted as strong suppression of charge fluctuations. We note that this primarily arises from the use of large Hubbard U (10 eV) together with density-density type of Coulomb interaction used in their work. This combination of -large U and absence of non-density-density terms- is expected to strongly enhance charge localization by suppressing dynamical charge fluctuations and drive large spectral weight transfer from the quasiparticle states[26]. Consequently, neglecting the non-density-density terms tends to strongly localize the low-energy states and overestimate the loss of partial $3d$ occupancy. Unlike their study, the smaller renormalization in our calculations using the full type with realistic U indicates a Hund's metal like regime rather than strongly localized charge-frozen state.

Correspondingly, the effect of increase in the strength of Hund's coupling i.e $J=0.0$ eV to 1.15 eV, is given on respective occupations in Table VI.

It can be inferred that the DFT calculations yield an approximate IS state ($t_{2g}^{4.62}e_g^{1.79}$) and even $J=0$ eV yields a pure IS state within the DFT+DMFT framework. When the Hund's coupling strength is increased to 1.15 eV the $3d$ configuration shows a finite contribution of the HS state as can be noted from the occupation, which is expected as Hund's coupling tends to favor maximum spin state ($t_{2g}^{4.06}e_g^{2.21}$) yielding a tendency towards HS configuration. Furthermore, with a strong Hund's coupling magnitude inherent to the system i.e. $J= 1.15$ eV, the analysis of its spin-state probability distribution suggests presence of mixed valence and

mixed spin-state configuration at 110 K- as histogram peaks near d^6 multiplet with substantial d^5 and d^7 weights, while the spin-state distribution shows broad dominant contributions from $S=1/2, 1$ & 2 (refer Fig 6. This suggests that magnetic moment does not arise from a single static spin-configuration but from a dynamical superposition of different atomic multiplets with an overall HS state favored by strong Hund's coupling ($J= 1.15$ eV) in the system. The mixed valence state with finite contributions from the several spin state multiplets suggests enhanced metal-ligand hybridization and spin-charge coupling in stabilizing the mixed-spin ground state. This is consistent with a recent cluster-multiplet study by Zheng et al, while studying the effect of epitaxial strain on $SrCoO_3$ thin films[51]. We note that at low temperatures the system exhibits characteristics suggestive of the Hund's metallicity by displaying an intermediate correlations regime with both the itinerant and localized limits. This is particularly evident from the large $\langle \Delta N^2 \rangle$ along with strong mass enhancements pointing to presence of heavy quasiparticles down to the lowest calculated temperature, 110 K.

TABLE V: Spin-orbital resolved mass-enhancement factor (m^*/m_{DFT}) along with quasiparticle spectral weight factor (Z) given in bracket, at $T= 110$ K for $J = 0, 0.6$ & 1.15 eV

J (eV)	$t_{2g} - up$	$e_g - up$	$t_{2g} - dn$	$e_g - dn$
0	1.45 (0.68)	1.27 (0.78)	1.41 (0.70)	1.27 (0.78)
0.6	2.44 (0.40)	2.00 (0.50)	1.83 (0.54)	1.89 (0.53)
1.15	7.13 (0.14)	6.24 (0.16)	1.88 (0.53)	5.46 (0.18)

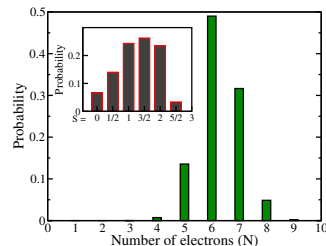


FIG. 6: Occupation probabilities of $3d$ - states at $T= 110$ K for $J=1.15$ eV. Inset displays probability distribution for different spin states at 110 K

TABLE VI: Orbital resolved occupancies of Co $3d$ states obtained using DFT and DFT+DMFT (at $T = 110$ K) methods

		t_{2g}	e_g
DFT		4.62	1.79
DFT+DMFT	$J = 0.00$	5.00	1.10
	$J = 0.60$	4.67	1.89
	$J = 1.15$	4.06	2.21

IV. CONCLUSION

In conclusion, a realistic account of the electronic correlations within the dynamical mean-field theory (DMFT) shows the presence of Hund's coupling dominated description of electronic structure properties of SrCoO₃. This is marked by strong orbital-selective intermediate range of quasiparticle mass renormalization and significant charge fluctuations. Notably, the agree-

ment of low temperature magnetization as well as the T_c value (considering the local nature of correlation effects in single-site DMFT) with the experimental results further confirms the Hund's coupling driven magnetism. The system exhibits a largely suppressed Fermi-liquid coherence scale of temperature lower than 100 K. We argue that the presence of large incoherency in both the e_g and t_{2g} orbitals of Co $3d$ manifold down to lowest calculated temperature rules out the possibility of conventional double-exchange like mechanism proposed for this system in previous studies. Our study shows that the local moment picture in this system stems from a mixed spin-state configuration comprised of dynamically fluctuating IS and HS states.

V. ACKNOWLEDGMENTS

We acknowledge the computational support provided by the High-Performance Computing (HPC) PARAM Himalaya at the Indian Institute of Technology Mandi.

-
- [1] D. E. Shai et al. Quasiparticle mass enhancement and temperature dependence of the electronic structure of ferromagnetic SrRuO_3 thin films. *Phys. Rev. Lett.* **110** (2013), 087004.
- [2] S. Moon et al. Dimensionality-controlled insulator-metal transition and correlated metallic state in $5d$ transition metal oxides $\text{Sr}_{n+1}\text{Ir}_n\text{O}_{3n+1}$ ($n = 1, 2$, and ∞). *Phys. Rev. Lett.* **101** (2008), 226402.
- [3] G. Cao and L. E. DeLong. Spin-orbit interactions in ruddlesden-popper phases $\text{Sr}_{n+1}\text{Ir}_n\text{O}_{3n+1}$ ($n = 1, 2$, and ∞) (2021).
- [4] Z. Wang et al. Dimensionality-driven insulator-metal transition in a-site excess non-stoichiometric perovskites. *Nat. Commun.* **1** (2010), 1, 106.
- [5] S. Bhardwaj and S.K.Pandey. Signatures of Hund's metal physics in the single-layered $3d$ transition metal oxide Sr_2CoO_4 . *Phys. Rev. B* **112** (2025), 125105.
- [6] S. Bhardwaj and S.K.Pandey. Correlation-induced metal to half-metal phase transition and large orbital moment in Sr_2CoO_4 . *Phys. Rev. B* **111** (2025), 075155.
- [7] Y. E. Putri et al. Bismuth-substituted $\text{Sr}_3\text{Ti}_2\text{O}_7$ ruddlesden-popper oxide prepared by molten salt method with tunable electrical conductivity. *Case Stud. Chem. Environ. Eng.* **8** (2023), 100513. ISSN 2666-0164.
- [8] M. Mochizuki and M. Imada. Magnetic and orbital states and their phase transition of the perovskite-type TiO_2 oxides: Strong coupling approach. *J. Phys. Soc. Jpn.* **70** (2001), 6, 1777.
- [9] S. K. Pandey et al. Investigation of the spin state of Co in LaCoO_3 at room temperature: Ab initio calculations and high-resolution photoemission spectroscopy of single crystals. *Phys. Rev. B* **77** (2008), 045123.
- [10] W. Sun et al. Electronic and transport properties in ruddlesden-popper neodymium nickelates $\text{Nd}_{n+1}\text{Ni}_n\text{O}_{3n+1}$ ($n = 1 - 5$). *Phys. Rev. B* **104** (2021), 184518.
- [11] J. Yang et al. Pressure-induced spin reorientation and spin state transition in SrCoO_3 . *Phys. Rev. B* **92** (2015), 195147.
- [12] H. Hsu and S. Huang. Simultaneous metal-half-metal and spin transition in SrCoO_3 under compression. *Phys. Rev. Mater.* **2** (2018), 111401.
- [13] J. G. J. Pérez, J. Blasco and J. Stankiewicz. Spin-Glass Behavior and Giant Magnetoresistance in the $\text{Ni}_{0.3}\text{Co}_{0.7}\text{O}_3$ (RE = La, Nd, Sm) System. *Phys. Rev. Lett.* **80** (1998), 11, 2401.
- [14] H. S. K. Takada, F. I. E. Takayama-Muromachi, R. A. Dilanian and T. Sasaki. A new superconducting phase of sodium cobalt oxide. *Advanced Materials* **16** (2004), 21, 1901.
- [15] D. Li et al. Superconducting dome in $\text{Nd}_{1-x}\text{Sr}_x\text{NiO}_2$ infinite layer films. *Phys. Rev. Lett.* **125** (2020), 027001.
- [16] R. S. Dhaka et al. Tuning the metal-insulator transition in NdNiO_3 heterostructures via Fermi surface instability and spin fluctuations. *Phys. Rev. B* **92** (2015), 035127.
- [17] I. Terasaki, Y. Sasago and K. Uchinokura. Large thermoelectric power in NaCo_2O_4 single crystals. *Phys. Rev. B* **56** (1997), R12685.
- [18] T. Ogawa et al. Electrical and magnetic properties and colossal magnetoresistance effect of $\text{La}_{1-x}\text{BixMnO}_3$. *Jpn. J. Appl. Phys.* **45** (2006), 11R, 8666.
- [19] Y. Long, Y. Kaneko, S. Ishiwata, Y. Taguchi and Y. Tokura. Synthesis of cubic SrCoO_3 single crystal and its anisotropic magnetic and transport properties. *J. Phys. Condens. Matter* **23** **24** (2011), 245601.
- [20] M. Kim and B. I. Min. Nature of itinerant ferromagnetism of SrRuO_3 : A dft+dmft study. *Phys. Rev. B* **91** (2015), 205116.
- [21] M. Hoffmann et al. Magnetic properties of defect-free and oxygen-deficient cubic SrCoO_3 . *Phys. Rev. B* **92** (2015), 094427.

- [22] S. Balamurugan et al. Specific-heat evidence of strong electron correlations and thermoelectric properties of the ferromagnetic perovskite $\text{SrCoO}_{3-\delta}$. *Phys. Rev. B* **74** (2006), 172406.
- [23] R. H. Potze, G. A. Sawatzky and M. Abbate. Possibility for an intermediate-spin ground state in the charge-transfer material $\text{SrCoO}_{3-\delta}$. *Phys. Rev. B* **51** (1995), 11501.
- [24] J. Kunepek, N. Parragh, G. Sangiovanni, A. Toschi and A. V. Kozhevnikov. Spin state of negative charge-transfer material. *Phys. Rev. Lett.* **109** (2012), 11.
- [25] S. Mathi Jaya, R. Jagadish, R. S. Rao and R. Asokamani. Electronic structure and magnetism of SrFeO_3 . *Phys. Rev. B* **43** (1991), 13274.
- [26] M. Aichhorn, S. Biermann, T. Miyake, A. Georges and M. Imada. Theoretical evidence for strong correlations and incoherent metallic state in SrFeO_3 . *Physical Review B* **82** (2010).
- [27] Y. Wang et al. Robust ferromagnetism in highly strained. *Phys. Rev. X* **10** (2020), 021030.
- [28] P. Blaha et al. Wien2k: An apw+lo program for calculating the properties of solids. *J. Chem. Phys.* **152** (2020), 7, 074101.
- [29] J. P. Perdew et al. Restoring the density-gradient expansion for exchange in solids and surfaces. *Phys. Rev. Lett.* **100** (2008), 136406.
- [30] F. Aryasetiawan et al. Frequency-dependent local interactions and low-energy effective models from electronic structure calculations. *Phys. Rev. B* **70** (2004), 195104.
- [31] M. Cococcioni and S. de Gironcoli. Linear response approach to the calculation of the effective interaction parameters in the LDA+U method. *Phys. Rev. B* **71** (2005), 035105.
- [32] X. Gonze et al. Recent developments in the abinit software package. *Comput. Phys. Commun.* **205** (2016), 106. ISSN 0010-4655.
- [33] K. Haule, C.-H. Yee and K. Kim. Dynamical mean-field theory within the full-potential methods: Electronic structure of CeIrIn_5 , CeCoIn_5 , CeRhIn_5 . *Phys. Rev. B* **81** (2010), 195107.
- [34] K. Haule. Exact double counting in combining the dynamical mean field theory and the density functional theory. *Phys. Rev. Lett.* **115** (2015), 196403.
- [35] F. Birch. Finite elastic strain of cubic crystals. *Phys. Rev.* **71** (1947), 809.
- [36] Z. Ali and I. Ahmad. Band profile comparison of the cubic perovskites CaCoO_3 and SrCoO_3 . *J. Electron. Mater.* **42** (2013), 438.
- [37] S. Nie, Y. Liu, Q. Liu, M. Wang and H. Wang. Phase transitions and thermal expansion of BaCoO_3 and SrCoO_3 up to 1413 k. *Eur. J. Mineral.* **29** (2017), 3, 433.
- [38] S. Balamurugan, M. Xu and E. Takayama-Muromachi. Magnetic and transport properties of high-pressure synthesized perovskite cobalt oxide $(\text{Sr}_{1-x}\text{Ca}_x)\text{CoO}_3$ ($0 < x < 0.8$). *J. Solid State Chem.* **178** (2005), 3431.
- [39] Z. Wu and R. E. Cohen. More accurate generalized gradient approximation for solids. *Phys. Rev. B* **73** (2006), 235116.
- [40] G. Kresse and J. Hafner. Ab initio molecular dynamics for liquid metals. *Phys. Rev. B* **47** (1993), 558.
- [41] T. Jia, Z. Zeng, H. Q. Lin, Y. Duan and P. Ohodnicki. First-principles study on the electronic, optical and thermodynamic properties of Abo_3 . *RSC Adv.* **7** (2017), 38798.
- [42] S. Balamurugan and E. Takayama-Muromachi. Structural and magnetic properties of high-pressure/high-temperature synthesized $(\text{Sr}_{1-x}\text{R}_x)\text{CoO}_3$ ($\text{R}=\text{Y}$ and Ho) perovskites. *J. Solid State Chem.* **179** (2006), 7, 2231. ISSN 0022-4596.
- [43] J. H. Lee and K. M. Rabe. Coupled magnetic-ferroelectric metal-insulator transition in epitaxially strained SrCoO_3 from first principles. *Phys. Rev. Lett.* **107** (2011), 067601.
- [44] M. Hoffmann et al. Magnetic properties of defect-free and oxygen-deficient cubic $\text{SrCoO}_{3-\delta}$. *Phys. Rev. B* **92** (2015), 094427.
- [45] W. Hai-Ping et al. Geometric and electronic properties of $\text{SrCoO}_{3-\delta}$: An LSDA+U study. *Chin. Phys. Lett.* **26** (2009), 1, 017105.
- [46] L. Vaugier, H. Jiang and S. Biermann. Hubbard u and Hund exchange j in transition metal oxides: Screening versus localization trends from constrained random phase approximation. *Phys. Rev. B* **86** (2012), 165105.
- [47] B. Amadon, T. Applencourt and F. Bruneval. Screened Coulomb interaction calculations: cRPA implementation and applications to dynamical screening and self-consistency in uranium dioxide and cerium. *Phys. Rev. B* **89** (2014), 12, 125110.
- [48] L. de' Medici. Hund's coupling and its key role in tuning multiorbital correlations. *Phys. Rev. B* **83** (2011), 205112.
- [49] J. M. Tomczak, K. Haule and G. Kotliar. Signatures of electronic correlations in iron silicide. *Proceedings of the National Academy of Sciences* **109** (2012), 9, 3243.
- [50] X. Deng et al. Signatures of mottness and hundness in archetypal correlated metals. *Nature Communications* **10** (2019).
- [51] X. Zheng et al. Mixed spin states for robust ferromagnetism in strained SrCoO_3 thin films. *arXiv:2508.01284*.

Supplementary material for "Hund's coupling driven nature of magnetism in negative charge transfer material, SrCoO₃"

Jyotsana Sharma^{1,3,*}, Shivani Bhardwaj¹, and Sudhir K. Pandey^{3†}

¹*School of Physical Sciences, Indian Institute of Technology Mandi, Kamand - 175075, India*

²*School of Mechanical and Materials Engineering,*

Indian Institute of Technology Mandi, Kamand - 175075, India and

³*Swami Vivekanand Govt. College Ghumarwin - 174021, India*

(Dated: December 14, 2025)

I. MOMENTUM-RESOLVED SPECTRAL FUNCTION PLOT ALONG WITH THE SPIN-ORBITAL RESOLVED DFT BAND-STRUCTURE

The Momentum resolved spectral function at temperatures 110 K and 300 K is displayed in Fig.1(b)& 1(c) respectively, along with the DFT calculated band structure shown in Fig. 1(a). The spectral function shows appreciable changes with temperature considering the quasiparticle peak positions of the low-lying e_g and t_{2g-up} (~ 1.5 eV below the E_f) states. The t_{2g-dn} channel spans a large bandwidth ranging from ~ 0.5 to 0.5 eV around the E_f and shows less thermal broadening

with increase in temperature from 110-300 K, which arises from a small effective U acting due to its large bandwidth, which apparently remains same as its DFT bandwidth- reflecting overall small renormalization from correlation effects and thermal broadening. Nevertheless, the loss of quasiparticle coherence is clearly visible (sharp features of spectral function signify coherency i.e. quasiparticle with large lifetime, whereas, broadened curves signify incoherency i.e. quasiparticle with shorter lifetime) with increase in temperature from 110 to 300 K for all other orbitals i.e. e_g manifold and t_{2g-up} channel, evident from narrowing of bandwidth and increase in degree of incoherency with the inclusion of correlation effects.

* jyotsana.sharma1290@gmail.com

† sudhir@iitmandi.ac.in

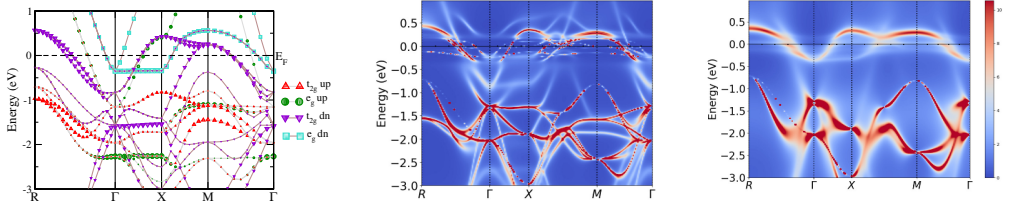


FIG. 1: (a) Orbital-resolved DFT band structure for Co- d . (b) Momentum-resolved spectral function at 110 K for $J = 1.15$ eV. (c) Momentum-resolved spectral function at 300 K.